

A Low-Cost Optical Approach to Evaluate the Life Time of Hall Thruster Discharge Channel

Wensheng Huang* and Alec D. Gallimore†

Plasmadynamics and Electric Propulsion Laboratory, Ann Arbor, MI 48109

This paper will present a novel procedure for performing accelerated wear test on Hall thruster discharge channels. The procedure takes advantage of a number of recent advances in optical diagnostics that have enabled increasingly accurate non-intrusive determination of both the length of the erosion zone and the erosion rate of the discharge channels in a Hall thruster. In the proposed procedure, two-axis laser-induced fluorescence is used to determine the energy and direction of the singly-charged ions responsible for the majority of the channel erosion. This data can then be used to determine the starting depth of the erosion zone inside the channel. It can also potentially be correlated to the angles of the chamfers at the end of the life of the channels. If it is determined that the predicted shape of the channels at the end of life intersect with the magnetic poles, an accelerated wear test can be performed to determine the amount of time to reach pole-exposure. This accelerated life test would involve the use of laser-induced fluorescence and cavity ring-down spectroscopy to accurately predict the change in the shape of the discharge channels in short time steps. The paper will describe in detail each step of this novel procedure, the assumptions made at each step, and the current body of scientific evidence that support these assumptions.

I. Introduction

THE biggest hurdle to flight for a typical Hall thruster system is the cost in time and resources related to flight qualification. To a Hall thruster designed for interplanetary mission, this hurdle is especially costly to overcome. For example, a Hall thruster could have yielded better performance on the Dawn mission¹ but none were selected due to the lack of demonstrated life.

The flight qualification of a Hall thruster can be a very involved process, as all of its components need to demonstrate the necessary life time (tens of thousands of hours). However, many of these components either have flight heritage or is based on a design with flight heritage. For example, many cathodes have been flown and do not necessarily need to be re-qualified when integrated with a Hall thruster. One of the most important thruster component that does need to be qualified, perhaps even on a per-mission basis, is the discharge channel walls. The community has traditionally characterized the end-of-life of the channel walls as the point when they become so eroded that the magnetic pole pieces they protect become exposed. This is often called the “soft failure” point. After this point, erosion of the magnetic pole pieces will alter the magnetic circuit and degrade thruster performance. This paper will focus on methods for experimental characterization of channel wall life time. Due to recent interest in developing high-power long-life Hall thrusters for interplanetary missions,² it is becoming more critical that we examine the flight qualification process and look for ways to cut resource and time costs.

Recent advances in optical diagnostics for the Hall thruster have led to the development of laser-induced fluorescence (LIF) velocimetry³ and cavity ring-down spectroscopy (CRDS)⁴ for studying discharge channel wall erosion. These advances give rise to new methods for evaluating the life time of channel walls at, potentially, a fraction of the expense and time when compared to traditional method. In particular, we are now able to accurately resolve the spatial location at which ions begin to accelerate along the channel wall. There is strong evidence that this location correlates with the start of the erosion band on the wall.³ We are also able to measure the density of sputtered boron in real time via CRDS and correlate that data to the sputter rate of the boron nitride channel walls.⁴

The proposed approach for evaluating channel wall life time takes advantage of the unique capabilities offered by LIF and CRDS. In phase I, the erosion zone location measured by LIF is combined with some method to conservatively estimate the end-of-life (EOL) eroded chamfer angle. One can then qualitatively determine whether the

* Presently Research Engineer, NASA Glenn Research Center, wensheng.huang@nasa.gov, AIAA Member.

† Arthur F. Thurnau Professor, Aerospace Engineering, alec.gallimore@umich.edu, AIAA Fellow.

magnetic poles will become exposed. Specific methods for estimating the EOL chamfer angle will be examined in the paper. This single-point-in-time measurement may be sufficient to determine whether a full wear test is needed or a partial wear test is sufficient to estimate the channel wall life time. Should a full wear test be determined to be necessary, the proposed approach proceed to phase II.

In phase II, LIF and CRDS measurements are combined to estimate short duration changes in the erosion band. Since LIF measurement give the start location of the erosion band and CRDS measurement give the volumetric sputter rate of the eroded material, the two measurements combined can be used to predict the shape of the channel a few hundred operational hours into the future. One would then reshape the channel based on the said prediction and take new LIF and CRDS measurements. This process is repeated in steps of few hundred operational hours until the pole pieces are exposed or the required life time is demonstrated.

The remainder of this paper will describe in detail this novel approach for qualifying Hall thruster discharge channel walls. The paper begin with a basic description of current approach to demonstrating Hall thruster channel life time. It will then describe the basic principles of and experimental setup for the optical diagnostics that form parts of the novel approach to measuring channel wall life. The paper will continue with a description of the said approach, a list of assumptions made, and a review of the scientific evidence supporting those assumptions. Towards the end, the paper will perform a simple cost analysis for cost and time savings associated with the novel approach as opposed to the traditional approach. Then, the paper will conclude with discussions of drawbacks and other life-time-related applications for the diagnostics described. Readers who are familiar with the traditional qualification, LIF velocimetry, and CRDS diagnostic can skip to Section IV.

II. Background

This section describes the theoretical background upon which the diagnostics described in this paper is built. All wavelengths are reported vacuum value and all intensities reported in arbitrary unit (a.u.) unless otherwise specified.

A. Traditional Method for Qualifying Hall Thruster Channel Wall

The simplest and most accurate approach to qualifying the channel walls of a Hall thruster is to simply operate it for enough hours to satisfy some mission requirement plus margin, or until failure. This approach is usually called the long duration wear test, or the long duration test (LDT). The LDT is usually designed to qualify the entire thruster, though discharge channel erosion is usually treated as the primary failure mechanism. Unfortunately, this is also the most expensive and time consuming approach. Furthermore, if the thruster channel does not meet the life requirement (perhaps because the magnetic field topology is slightly different from the design, or the material is slightly different from the specifications) one will usually not know until the LDT is well underway. To aid in the assessment of the erosion of the discharge channel, profilometry is often employed to measure the discharge channel profiles and compute the erosion rate.^{5,6}

There are at least four published examples of the traditional approach to performing a Hall thruster LDT where the duration is longer than 5,000 hours. The SPT-100, a Russian-made 1.35-kW thruster, was independently wear tested by Fakel⁷ for 7,000 hours and the Jet Propulsion Laborator (JPL) for 5,730 hours.⁸ The PPS1350-G, a European-made 1.5-kW thruster, was tested by Snecma for 10,500 hours.⁹ The BPT-4000, a U.S.-made 4.5-kW thruster, was tested by Aerojet for 10,400 hours.¹⁰ In these tests, the primary erosion diagnostics were photography and profilometry. At the end of each of these tests, the test article shows radial grooves that appear at semi-regular azimuthal interval on the chamfered part of the discharge channel. Figure 1 shows an example of these grooves on the BPT-4000 tested by Aerojet.¹⁰

In the next two section, we will describe the optical diagnostics that will form the basis for the novel low-cost approach for evaluating Hall thruster channel life.

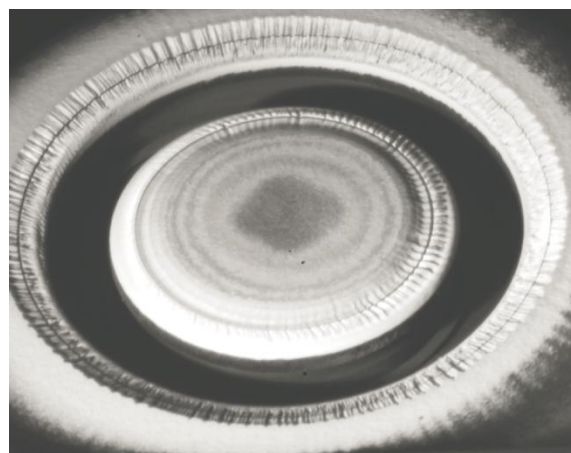


Figure 1. In-situ photograph of the BPT-4000 at 10,400 hours of operation.¹⁰

B. Laser-Induced Fluorescence

This section briefly describes how laser-induced fluorescence (LIF) can be used to obtain ion velocity distribution function (VDF). This data can be used to locate, in-situ, the start location of the acceleration zone, which is correlated with the start location of the erosion zone. When an atom is moving in the direction of a photon's wave vector, the atom absorbs the photon at a shifted frequency due to the Doppler effect. By varying the frequency of the injected laser light and measuring the intensity of the collected fluorescence one can construct the velocity distribution function of the atom population. The atom velocity, v , can be calculated from the shift in frequency using Eq. (1),

$$\frac{\nu_1 - \nu_0}{\nu_0} = -\frac{v}{c} \quad (1)$$

where ν_1 is the laser frequency, ν_0 is the at-rest absorption frequency, v is the particle velocity, and c is the speed of light.

The Xe II 835.0 nm LIF scheme is a particularly useful scheme for measuring the kinetic energy of the ions in the discharge channel. Figure 2 shows the transition diagram for this scheme. This LIF scheme has several advantages. One, it is accessible by a relatively inexpensive diode laser. Two, under certain circumstances, the hyperfine structure can be ignored while increasing the measurement uncertainty by a negligible amount.^{11, 12} Third, the lower state of the Xe II 835.0 nm transition is metastable and the LIF scheme is non-resonant. Fourth, the transition is generally not saturated for a typical LIF experiment.^{3, 13}

Note the population measured by LIF is of the lower state of the transition. Since there are no physical forces in the Hall thruster that distinguish between the various energetic states of a species, one can assume that the lower state of the transitions has the same VDF as all of the other states of the associated species

C. Cavity Ring-Down Spectroscopy

Cavity ring-down spectroscopy (CRDS) is a very sensitive form of absorption spectroscopy that can be used to measure the density of sputtered product. Berden, Peeters, and Meijer wrote a great review of recent development in the use CRDS as a diagnostic.¹⁴ CRDS operates on the principle that by sending a beam of photons through an absorber and measuring the change in intensity, one can obtain the absolute line-integrated density of the absorber. CRDS differs from traditional absorption spectroscopy in that a cavity, formed from a pair of highly reflective mirrors, is used to trap light. Instead of one pass, the trapped photons make many passes through the absorbing medium. Each time the trapped light strikes one of the mirrors, a small fraction of it leaks out. The intensity of the leaked light is measured by a detector. When the light source is a continuous-wave laser, the beam is extinguished (e.g. with an acousto-optical modulator), and then the light within the cavity will begin to decay in intensity. The characteristic time constant of the decaying signal measured by the detector can then be used to calculate the absolute line-integrated density of the absorber inside the cavity. Figure 3 illustrates the operational principles of CRDS. The grey arrow pointing from the detector to the acousto-optical modulator (AOM) indicates a feedback signal that commands the AOM to cut off the laser beam.

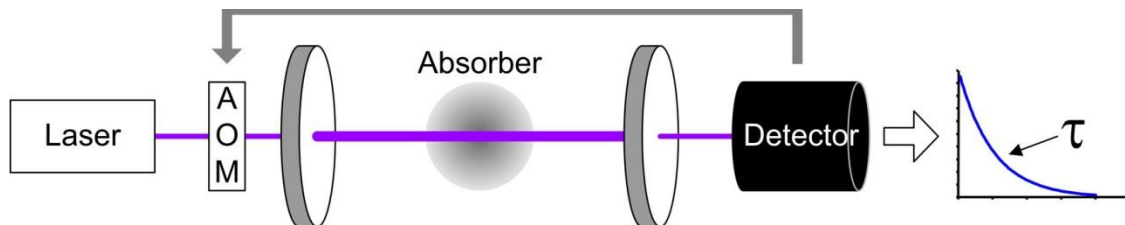


Figure 3. Operational principles of cavity ring-down spectroscopy.

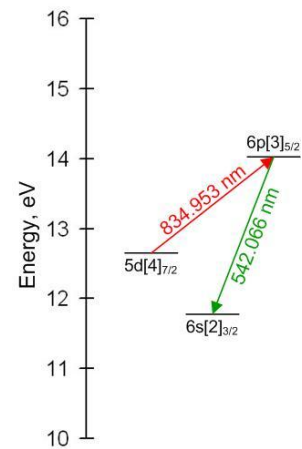


Figure 2. Transition diagram for the Xe II 835.0 nm (vac) LIF scheme.

Equations (2) and (3) govern the ring-down behavior and time constant in a typical cavity,

$$S(t, \nu) = S_0 \exp[-t/\tau(\nu)] \quad (2)$$

$$1/\tau(\nu) = \frac{c}{L} \left[\int k(x, \nu) dx + (1 - R_M) \right] \quad (3)$$

where S is the signal intensity, S_0 is the initial signal intensity, τ is the characteristic time of decay, also called the ring-down time, L is the cavity length defined as the distance between the two mirrors, R_M is the mirror reflectivity, and $k(x, \nu)$ is the absorption coefficient at a given laser frequency ν and position along the cavity optical axis x and the integral term represents the line-integrated contribution from the absorber. In practice, the mirror reflectivity changes in time and there is a scattering effect that decreases the effective reflectivity. To extract absolute line-integrated density, the ring-down time is compared to the empty cavity ring-down time, τ_0 . This is shown in Eq. (4),

$$\text{Abs}(\nu) \equiv \int k(x, \nu) dx = \frac{L}{c} \left[\frac{1}{\tau(\nu)} - \frac{1}{\tau_0} \right] \quad (4)$$

where Abs is the sample absorbance and is unitless. By scanning the laser frequency across an entire transition line, one can then integrate for the total absorbance and relate it back to the absolute density of the lower state of the transition being studied. Equation (5) shows this relationship,

$$\int n_1 dx = 8\pi \frac{g_1}{g_2} \frac{\nu_{21}^2}{A_{21} c^2} \int \text{Abs}(\nu) d\nu \quad (5)$$

where n is absolute density, g is level degeneracy, ν is transition frequency, A is the spontaneous emission rate, subscript 1 denotes lower state, and subscript 2 denotes upper state.

Since recent Hall thruster designs typically feature boron nitride (BN) channel walls, the B I 249.848 nm transition is currently the best candidate for use with CRDS. While nitrogen is a sputtered produce from BN channel walls, it is not a good choice for optical measurement because of the presence of trace amount of background nitrogen leaking into any given vacuum facility. Of the available boron lines, B I 249.848 nm transition has two advantages. One, it is one of a doublet of ground state transitions and most of the boron are expected to be born into the ground state.¹² Two, the intensity of this transition is the higher of the two transitions that form a doublet by a factor ~ 2 . Fig shows the transition digram for the B I 249.848 nm transition.

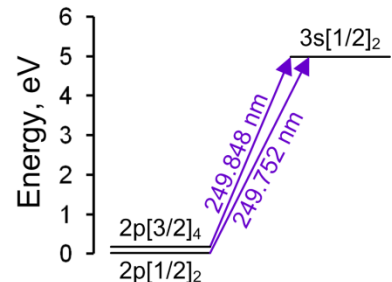


Figure 4. Transition diagram for the B I 249.848 nm (vac) transition.

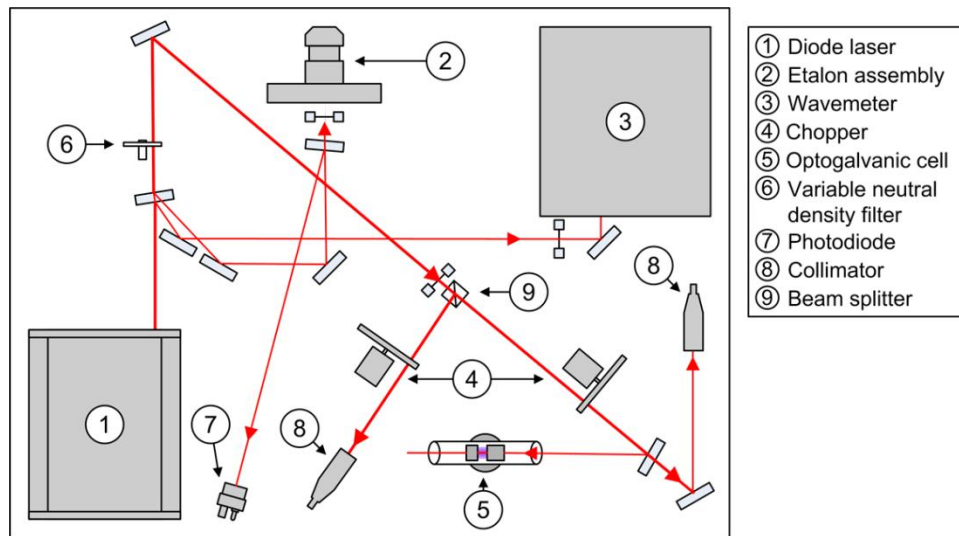


Figure 5. Air-side experimental setup for the two-axis near-wall LIF study.

III. Experimental Setup

As previously mentioned, the novel optical approach to accelerated wear testing is based on new advances in LIF and CRDS diagnostics. This section briefly describes the setup of the tests that made those advances as examples of how the test equipment can be set up. An implementation of the optical approach to accelerated wear testing does not require these exact diagnostic setup, only the key elements that are central to obtaining the specified data.

A. Laser-Induced Fluorescence Setup

The original purpose of the two-axis near-wall ion LIF study is to characterize the energy distribution function of the ions that bombard the channel walls. It is discovered, in the course of performing the study, that the technique also measures the starting location of the acceleration zone very accurately. Figure 5 shows the air-side laser and optics setup for this LIF study. The laser system used in this study is a tapered-amplified diode laser. This system has a nominal linewidth of ~ 10 MHz and a mode-hop-free range of ~ 12 GHz. The total output power is ~ 250 mW.

Since the key measurement to be obtained by LIF is the ion energy, the stationary reference used compute the shift in transition frequency is very important. This setup uses an etalon assembly (2-GHz free spectral range, finesse >250), a wavemeter (± 1 pm) and an optogalvanic cell to establish the stationary reference. The input beam for the cell is mechanically chopped at ~ 1.1 kHz. The cell is filled with approximately 3 Torr of xenon and 4 Torr of neon. The ends of the cell are angled at approximately 10 degrees from being perpendicular to the laser beam to prevent retro-reflection. The output signal is fed to a lock-in amplifier. The optogalvanic cell is operated at 250 V.

To fully capture the energy and angle of the bombarding ions, two laser beam injected at different angle is needed. The main beam from the laser source is split roughly 50:50 by a non-polarizing beam splitter cube. The two output beams are each mechanically chopped at a different frequency before being collimated into optical fibers. The fibers deliver the light through feedthrus into the vacuum chamber. About 20 mW in total laser beam power is delivered to the interrogation zone. The corresponding beam intensity is ~ 25 mW/mm².

Figure 6 shows a diagram of the vacuum-side experimental setup for the LIF study. The injection optics are fixed to the floor of the chamber while the thruster is mounted on a pair of motion stages. Subplot (a) shows how the two sets of injection optics are aligned with respect to the thruster for probing near the inner channel wall. Shown in dash outline is the position of the near-radial injection optics when probing near the outer channel wall. The near-radial injection optics is so named because it sends in laser light at a $60 \pm 1^\circ$ angle with respect to the thruster axis, which is close to but is not perfectly radial injection. Although analysis will be more complicated with a near-radial scheme, it is necessary for the laser light to reach to inside of the thruster channel. The beams are focused down to a point with a 1-mm diameter circular cross section via anti-reflect-coated plano-convex lenses. The injection beam focusing cones have half-angles of $\sim 0.5^\circ$ and the injection axes are aligned to within 0.1° using laser tools so cosine errors are negligible. The interrogation zone is at the 9 o'clock position when viewing the thruster face on.

For this LIF experiment, polarizers (not shown in the diagram) are placed between the optical fiber outputs and the lenses to control the beam polarization with respect to the local magnetic field direction. Doing this minimize the Zeeman effect, which can distort the apparent energy distribution function. This step is only important if one wants

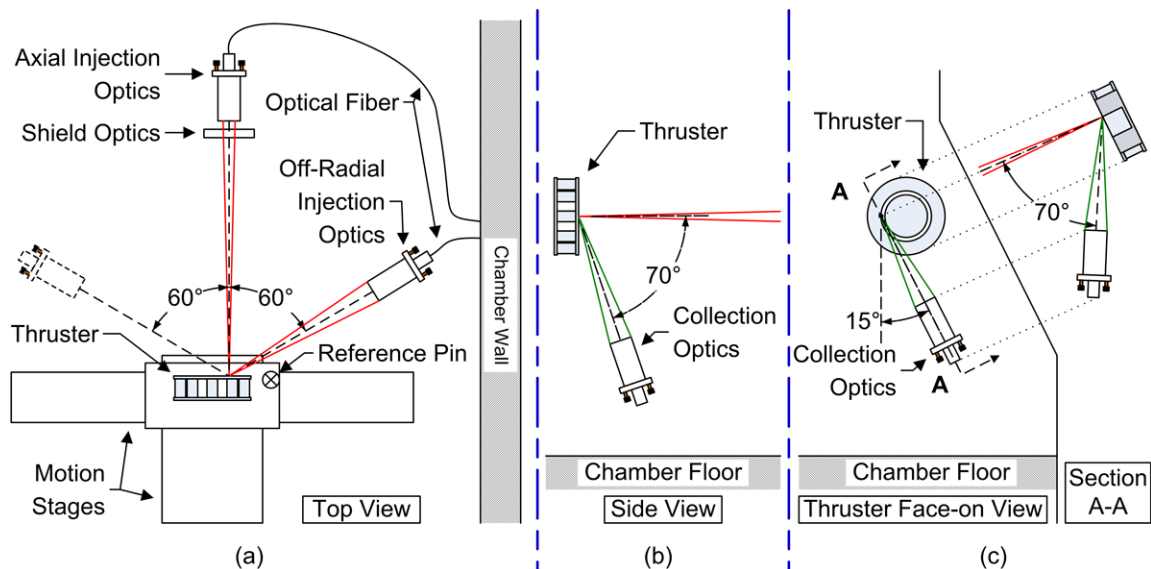


Figure 6. Vacuum-side experimental setup for the two-axis near-wall LIF study.

an accurate measurement of the ion energy distribution function. Since the Zeeman effect induces no net frequency shift, mean velocity measurement can be carried out even if the Zeeman effect is not accounted for.^{12, 15}

Figure 6 subplots (b) and (c) show the collection optics positions used to collect data from near the inner and the outer channel walls, respectively. The axial injection beam is shown for reference. The collection optics was built from a matching pair of anti-reflect-coated achromatic lenses. To counter the overall system thermal drift, a reference pin with a 1-mm-diameter hemispherical head is installed to the left of the thruster when viewed face on. The exact position of the head of this pin relative to the thruster is known and the reflected laser signal from this pin is used to compensate for thermal drift. Additionally, the yaw movement of the axial injection optics is motorized with a micro-stepper motor because this movement axis was found to undergo the most thermal drift during testing. The collection optics axis is set at a 70 ± 0.5 degree angle with respect to the thruster axis to allow the interrogation of the inside of the thruster channel. The interrogation volume resulting from the intersection of the injection and collection optics is a sphere of ~ 1.5 mm in diameter. Data is taken every 2 mm near the channel walls. Based on these two numbers, the uncertainty on the start location of the near-wall acceleration zone is limited by the axial data resolution to ± 1 mm. However, ± 0.5 mm is easily achievable with slight refinement to the setup.

Figure 7 shows a photograph of the vacuum-side experimental setup for the LIF test. Greater detail regarding the two-axis near-wall ion LIF study can be found in these papers.^{3, 12}

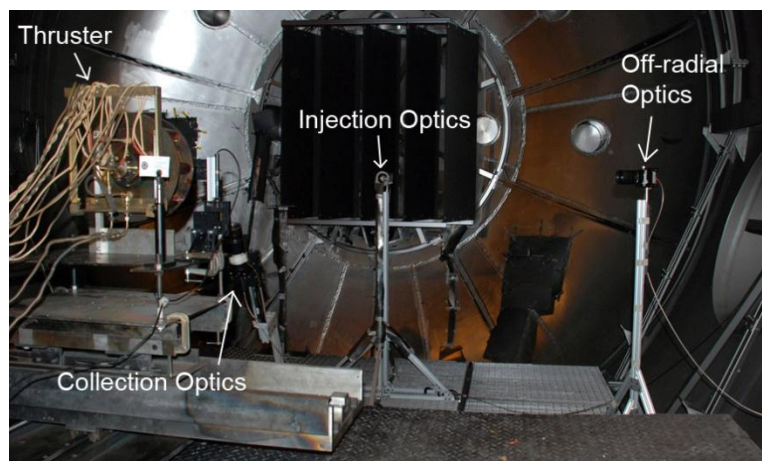


Figure 7. Photograph of the vacuum-side setup for the two-axis near-wall LIF study.

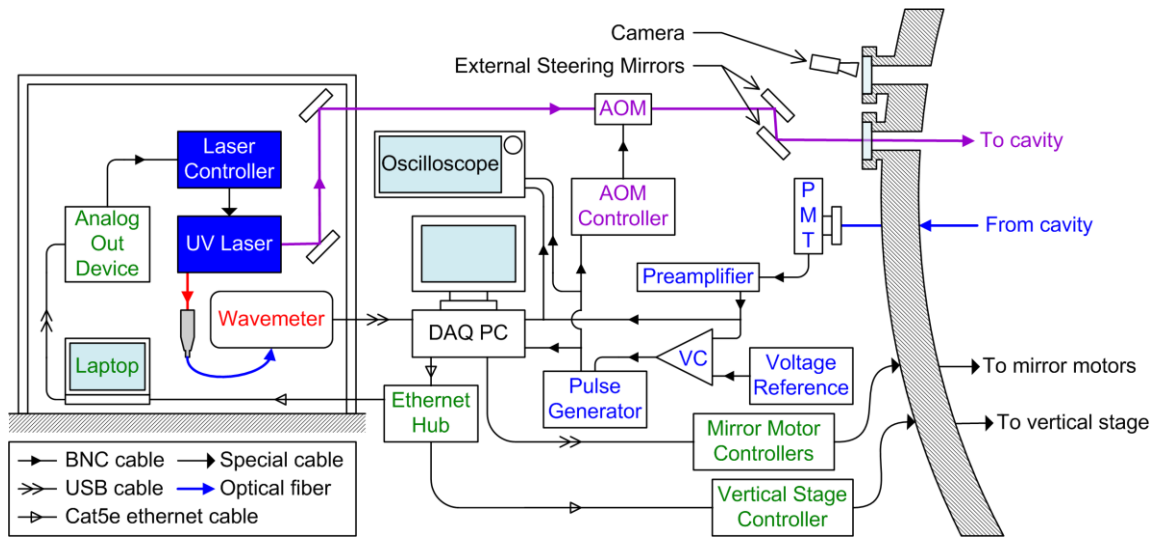


Figure 8. Air-side experimental setup for the CRDS study.

B. Cavity Ring-Down Spectroscopy Setup

The CRDS test described here is the initial demonstration of the use of this technique to measure in-situ the discharge channel sputter rate. Figure 8 shows the air-side experimental setup for the CRDS study. The laser system used in this study is a frequency-quadrupled diode laser and is comprised of three components. The first component is a taper-amplified diode laser that typically outputs ~ 500 mW of 1000-nm light. The second component is a frequency-doubling cavity in a bow-tie configuration that takes the 1000-nm light and frequency-doubles it to ~ 170 mW of 500-nm light. The third component, shown in Fig. 9, is another frequency doubling cavity in a bow-tie configuration that frequency-doubles the 500-nm light to ~ 10 mW of 250-nm light. The linewidth of the 250-nm laser output is ~ 4 MHz. This UV laser is housed in a laser room to protect it from the dust and noise in the rest of the facility.

For stationary reference, a small amount of the ~ 1000 nm laser light generated by the first laser component is split off and coupled into a Fizeau-type wavemeter. The wavemeter has an accuracy of ± 60 MHz at 1000 nm, or ± 0.2 pm, and a resolution of 10 MHz. The wavelength of the frequency-quadrupled light is calculated from this reading by simply dividing by 4, which gives an accuracy of ± 0.05 pm at 250 nm. During the CRDS test, to excite resonance in the CRDS cavity, the UV laser continuously executes triangular sweeps at a rate of ~ 0.25 pm/s over a range of ~ 0.25 pm at the 250-nm output.

The UV laser beam exiting the laser first passes through an acousto-optic modulator (AOM). Roughly 70% of the input beam power is coupled into the first order mode of the AOM output. The first-order beam is then injected into the vacuum chamber to the CRDS cavity via external steering mirrors. The output from the CRDS cavity is returned via optical fiber to a photomultiplier through a band-pass interference filter with a 10-nm bandwidth centered at 250 nm. The photomultiplier current is converted to voltage via a preamplifier. The output from the preamplifier is fed to the data acquisition computer (DAQ PC) and a voltage comparator circuit. The voltage comparator circuit is built into a Schmitt trigger configuration and has a switching time of 20 ns. The reference voltage for this circuit is provided by a battery. This circuit drives a pulse generator that has an insertion delay of 60 ns. The pulse width is set to 12 μ s, which is more than ten times the typical ring-down time. Output of the pulse generator is fed into the AOM controller to initiate ring-down when the voltage comparator decides the signal in the cavity is high enough. This output pulse is also fed into the DAQ PC to trigger the start of data acquisition.

Figure 10 shows the vacuum-side experimental setup for the CRDS study. The thruster is mounted on a vertical motion stage while the CRDS cavity is fixed to the floor through a set of vibration isolators. The physical structure for the cavity is made from four hollow aluminum square tubes welded together. This design provides the necessary

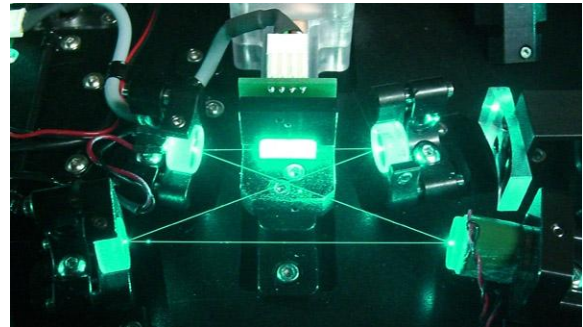


Figure 9. Second frequency-doubling stage in the UV laser.

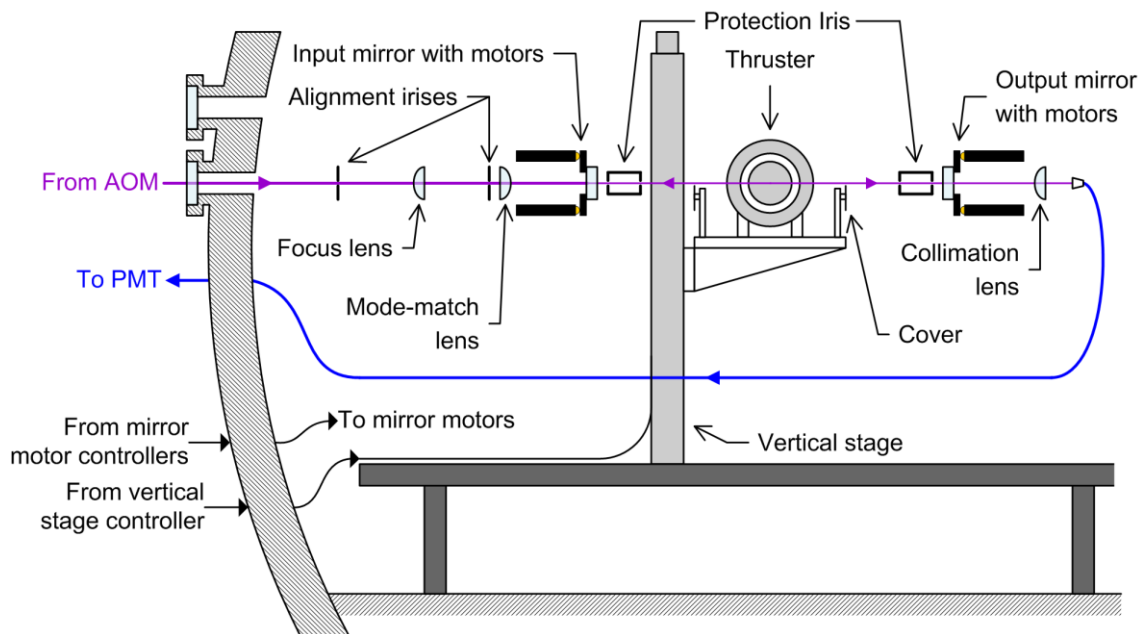


Figure 10. Vacuum-side experimental setup for the CRDS study.

structural rigidity to maintain the relative position of the two cavity mirrors. Thermal expansion was found to not be an issue during a thermal environment test. The first-order beam from the AOM is coupled through a set of alignment guides, a set of mode-matching lenses, and into the mirror pair that forms the CRDS cavity. The mode-matching lenses couples most of the laser into the TEM₀₀ mode of the CRDS cavity. The mode-matching lenses couples most of the laser into the TEM₀₀ mode of the CRDS cavity. The cavity mirrors are custom fabricated by a specialized mirror coating company. These mirrors are made from 1" diameter, 1/4" thick super-polished fused silica substrate. One side of each mirror is concaved with a 1-m radius-of-curvature and coated for high reflectivity at ~250 nm. The other side is flat and uncoated. The CRDS cavity beam resides at 4.0 ± 0.5 mm axially downstream of the thruster channel exit plane and has a beam waist of 0.2-0.25 mm. The mirrors sit on kinematic stages that have been modified to have motorized tilt and yaw motion. These motors are needed to keep the CRDS cavity in alignment during pumpdown and between acquisition of data sets. Additional protective iris and covers are also present to minimize the amount of particles depositing on the cavity mirrors. The covers also act as positional reference for in-situ position checks. Figure 11 shows a photograph of the vacuum-side setup.

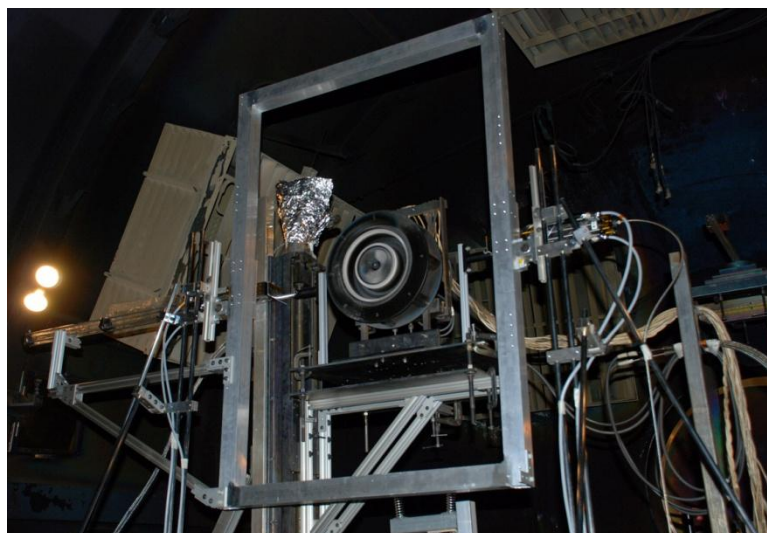


Figure 11. Photograph of the vacuum-side setup for the CRDS study.

IV. The Approach

This section will begin by describing the proposed approach for accelerated discharge channel qualification. It will list important assumptions and supporting evidence from the LIF and CRDS tests as well as the literature. The section will perform analysis of how the measurement uncertainty influences the overall uncertainty of the life time assessment. It will also list alternate diagnostics that can provide similar data.

A. Qualitative Life time Assessment via LIF

The optical approach to Hall thruster discharge channel life time assessment is divided into two phases. The purpose of phase I is to make a qualitative assessment of whether the discharge channel wall can become eroded enough to expose the magnetic circuit. If the magnetic circuit can become exposed, phase II is used to determine the time between the start of thruster operation and the exposure of the magnetic circuit. Phase I is relatively short and inexpensive compared to phase II, which is relatively short and inexpensive compared to a traditional LDT.

Phase I begins by using LIF to measure the near-wall axial location at which the ion energy exceeds a pre-defined threshold. This location will be referred to as the start location of the near-wall acceleration zone. This particular location is chosen based on two assumptions related to Hall thruster channel wall erosion. The first assumption is that erosion of boron nitride by xenon bombardment only occurs when the xenon energy exceeds a certain threshold. This threshold energy can then be translated to an energy level that near-wall ions (pre-sheath) must have to cause erosion when it reaches the wall (post-sheath). This assumption has been proven to be valid in a number of ion gun studies¹⁶⁻¹⁸ as well as in-situ Hall thruster tests.^{3, 19} The second assumption is that the start location (upstream location) of the erosion band along the channel wall is radially aligned with the start location of the near-wall acceleration zone. This assumption can be made because electric potential lines up well with magnetic field lines in the discharge channel and magnetic field lines are mostly radial.²⁰ This alignment is not perfect, so measuring the start location of the acceleration zone as close as possible to the wall gives the best indication of where the erosion zone starts. The second assumption is supported by findings from the two-axis near-wall LIF study.³ Figure 12 shows the axial velocity distribution functions from near the outer wall of a 6-kW Hall thruster operating at a discharge voltage of 300 V and a discharge current of 10 A. Also shown in the figure is a sub-plot of where LIF data was taken and what the local channel wall profile looks like. The wall profile was measured via a profilometer prior to the LIF test. From this figure, one can see that the start location of the near-wall acceleration zone as previously defined correlates well with the start location of the erosion band.

The biggest weakness in the second assumption for the phase I measurement is that it is presently difficult to determine whether the start location of the the near-wall acceleration zone (and erosion band) remains fixed throughout the life of a Hall thruster. Figure 13 reproduces a figure from a paper by Absalamov, S. K., et al., that shows the channel wall profiles of the SPT-100 during 4000 hours of qualification testing.²¹ The start location of the erosion band appear roughly constant throughout the test and channel wall erosion progress by expanding in the radial direction.

Another measurement technique that can measure the start location of the erosion band is embedded wall

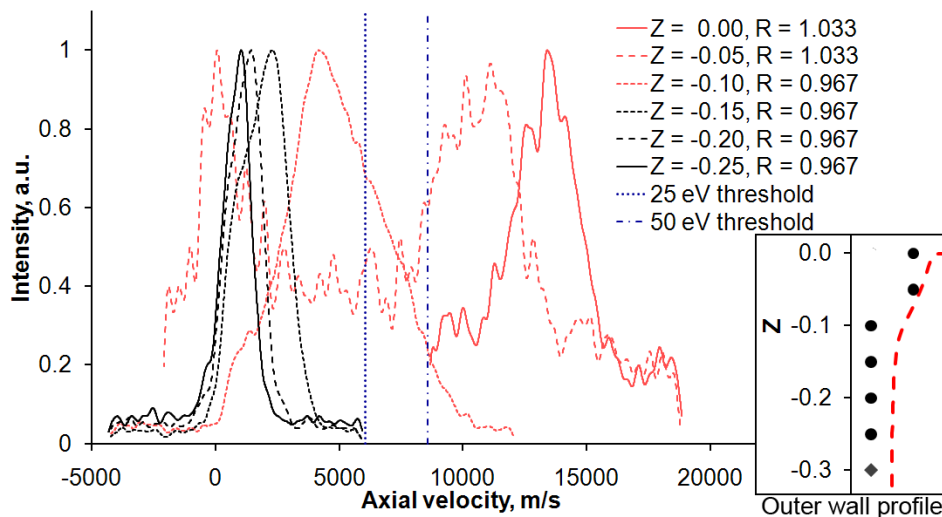


Figure 12. Axial velocity distribution functions from near the outer wall of a 6-kW Hall thruster operating at a discharge voltage of 300 V and 10 A.

probes.¹⁹ The main advantages of using wall probes are that the implementation is cheaper than performing LIF and the wall probes can also measure plasma temperature. The main disadvantages of using wall probes are that one needs to modify the discharge channel and the measurement accuracy is lower than LIF.

The second step in phase I is to estimate the end-of-life (EOL) angle of the eroded chamfer. Here, the definition of EOL varies depending on mission requirements but is typically 10,000+ hours or the terminal channel profile, if one exists. There are at least four ways to predict the chamfer angle, the first two of which are based on physical measurements.

The first method is to correlate the chamfer angle to plume divergence. Based on the geometry of plume expansion, one may expect the end-of-life chamfer angle to be related to how spread out the plume is. Thus, it may be possible to correlate the EOL chamfer angle to either near-field Faraday probe measurements or far-field Faraday probe measurements. At this point in time, there is insufficient data to determine whether this approach is viable.

The second method for estimating EOL chamfer angle is to use the two-axis near-wall LIF measurement to determine the direction and spread of the ions that bombard the wall. Assuming the EOL chamfer angle is determined by the path that the ions carve out, the angle of the near-wall ions should be an excellent indicator of that path. The biggest weakness of this method is that it is unclear whether the direction of the near-wall ions remain unchanged as the erosion of the channel walls progress.

The third method is to use past erosion profile data to create an empirical model for predicting EOL chamfer angle. This method would require a large number of prior tests and may be prohibitively expensive.

The fourth method is to conservatively assume that the EOL angle is at most 90° with respect to the firing axis. This is the same as assuming the amount of erosion caused by ions that are moving axially upstream (e.g. from backscattering) cause a negligible amount of erosion. It is the most conservative assumption that can be made on the EOL angle and requires no additional experimentation or analysis. However, this method may be too conservative for certain applications.

Note that for any of the proposed methods, the estimate can be easily made more conservative by adding margin to the EOL prediction.

Once both the start locations of the erosion bands and the EOL chamfer angles are known, one can predict the EOL channel profile and qualitatively assess the channel life time. If the predicted EOL channel profile intersects the magnetic circuit then quantitative life time assessment needs to be performed. Figure 14 shows a diagram of the concept behind the qualitative life time assessment. In this diagram, two possible magnetic pole piece positions are shown. If the pole piece is not intersected by the predicted eroded chamfer angle, then the mission requirement is satisfied. If the

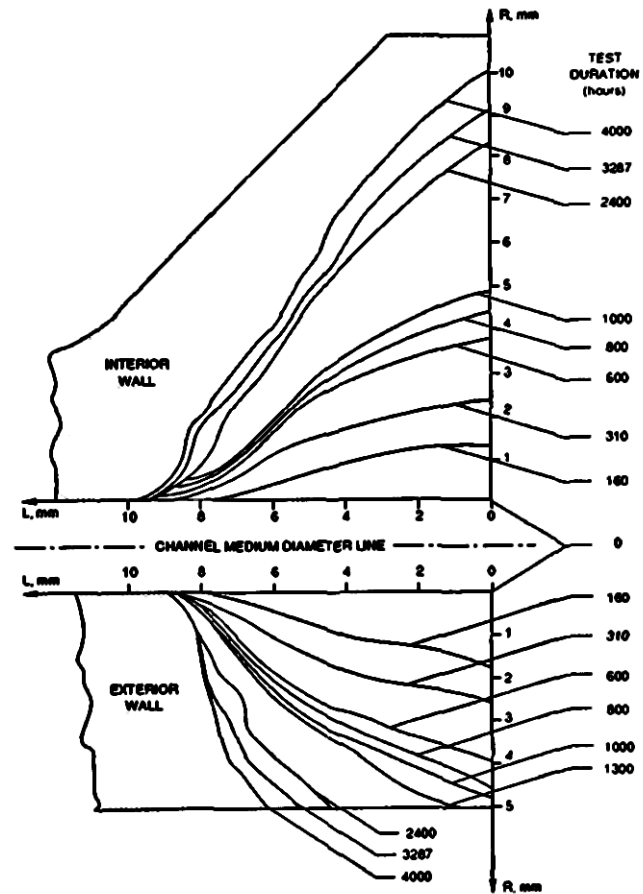


Figure 13. Reproduction of a figure showing SPT-100 erosion profiles during 4000 hours of life testing.²¹

whether the direction of the near-wall ions remain unchanged as the erosion of the channel walls progress.

The third method is to use past erosion profile data to create an empirical model for predicting EOL chamfer angle. This method would require a large number of prior tests and may be prohibitively expensive.

The fourth method is to conservatively assume that the EOL angle is at most 90° with respect to the firing axis. This is the same as assuming the amount of erosion caused by ions that are moving axially upstream (e.g. from backscattering) cause a negligible amount of erosion. It is the most conservative assumption that can be made on the EOL angle and requires no additional experimentation or analysis. However, this method may be too conservative for certain applications.

Note that for any of the proposed methods, the estimate can be easily made more conservative by adding margin to the EOL prediction.

Once both the start locations of the erosion bands and the EOL chamfer angles are known, one can predict the EOL channel profile and qualitatively assess the channel life time. If the predicted EOL channel profile intersects the magnetic circuit then quantitative life time assessment needs to be performed. Figure 14 shows a diagram of the concept behind the qualitative life time assessment. In this diagram, two possible magnetic pole piece positions are shown. If the pole piece is not intersected by the predicted eroded chamfer angle, then the mission requirement is satisfied. If the

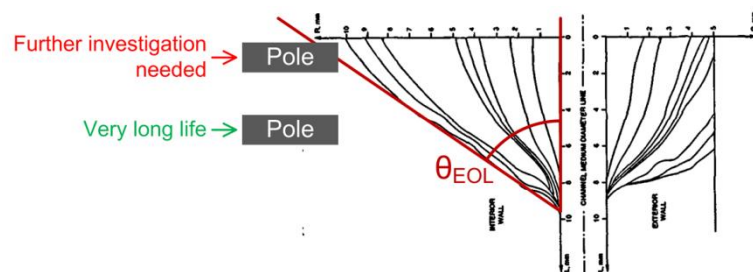


Figure 14. Diagram depicting the qualitative life time assessment. Discharge channel profiles of the SPT-100 are reproduced from a paper by Absalamov, S. K., et al.²¹

pole piece is intersected by the predicted eroded chamfer angle, quantitative life time analysis will need to be carried out in order to determine how long until pole piece is exposed. Note that for large-scale Hall thruster projects, even if a full qualification must be performed, it is better to perform a qualitative life time assessment first to ensure that the discharge channels of a given design have a good chance of surviving the qualification.

B. Quantitative Life time Assessment via LIF and CRDS

If it is found during the qualitative life time assessment that the discharge channel erosion profile may eventually intersect the magnetic circuitry, the optical approach to qualification will move into phase II. Phase II is the accelerated wear test of the discharge channel, also called the quantitative life time assessment within this paper.

The first step of phase II is to determine the start location of the erosion band. This step is the same as the first step of phase I. As such it does not need to be repeated if already performed. Phase II involves iterating a set of steps multiple times until the magnetic circuit is exposed. If the start location of the erosion band does not change over time as was assumed during phase I, it is not necessary to repeat this step. On the other hand, if the start location of the erosion band does change with thruster operation, this first step will need to be repeated as necessary. See the previous section for details on how to measure the start location of the erosion band.

The second step of phase II is to measure the erosion rate of each discharge channel. The proposed approach will use CRDS to determine in-situ and in a matter of hours the erosion rate. The erosion profile is assumed to be a straight chamfer, that is the eroded region has a triangular cross section. The assumption about the erosion profile being a straight chamfer is imperfect. From Fig. 13, one can see that the discharge channel profiles of the SPT-100 are typically shaped like an “S”. However, from Fig. 14, one can also see that after 4000 hours of operation, the channel wall profile align surprisingly well with a straight line. In the absence of a method to predict the exact curvature of the “S” shapes, the channel wall profiles are approximated as straight lines. Given the start location of the erosion band from the first step and the erosion rate from the second step, simple geometry can be applied to make a short time-step prediction of the change in the discharge channel profile.

The third step of phase II is to modify the discharge channel to match the shape predicted by the first two steps. Care must be taken to ensure the time steps are small enough to accurately capture the evolution of the discharge channel. The three steps of phase II are then repeated until the magnetic circuit is exposed or until mission duration plus margin is reached.

To assess the fidelity with which this accelerated discharge channel wear test captures the real discharge channel erosion profile, we will now use the SPT-100 erosion data from a paper by Absalamov, S. K., et al.,²¹ to analyze what kind of results would have been generated had the SPT-100 been put through the accelerated wear test. Figure 15 reproduces a plot showing the erosion rate of the SPT-100 as a function of operating hours.²¹ From this figure, it is apparent that for the first ~800 hours of thruster operation the erosion rate changed rapidly, but, after ~800 hours, the erosion rate changed much more slowly. We will begin by approximating the erosion rate as a function of operating hours using two linear fits. The result of the fit will be treated as the “real” erosion rate of the SPT-100 as a function of operation time. We define the eroded volume as the volume of material removed by erosion at a given time. The eroded volume can be calculated by integrating the erosion rate over time. Then, a function can be written to output the erosion rate for a given eroded volume. This function can then be used to predict what erosion rate will be measured by the CRDS sensor for a given eroded state that the discharge channel is in. This function is valid as long as the Hall thruster always have the same erosion rate for a given eroded profile regardless of how the thruster arrives at that profile.

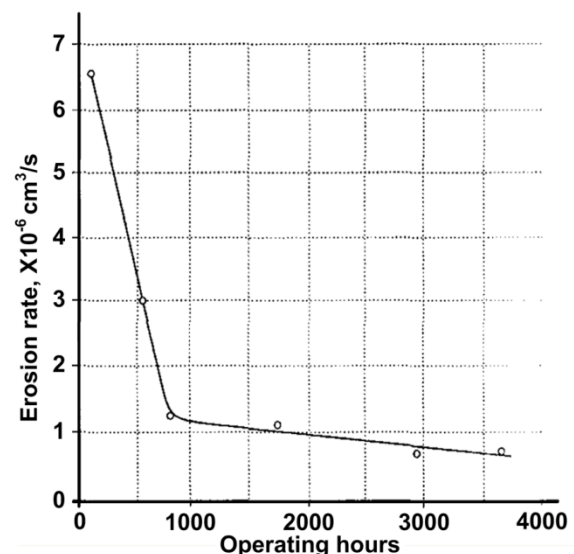


Figure 15. Reproduced plot of erosion rate as a function of operating hours for the SPT-100.

Figure 16 shows the erosion rate as a function of the eroded volume. The data is divided into two segments, one for each of the apparently linear regime from the erosion rate versus operating hours plot (Fig. 15). The curve fits shown in Fig. 16 are derived by performing integration and substitution with the linear fits to each segment in the erosion rate versus operating hours plot. These curve fits take on the form in Eq. (6),

$$ER(S) = \sqrt{b^2 + 2m(S - C)} \quad (6)$$

where ER is the erosion rate and S is the eroded volume. m and b are constants obtained from performing linear fits to each segment in the erosion rate versus operating hours plot. m is the slope and b is the intercept. C is a fitting constant that is equal to 0 for segment 1. We can now assess the fidelity of performing accelerated discharge channel wear test.

Figure 17 shows the results of a simulate discharge channel wear test of the SPT-100 where the time step is selected to be a fixed 300 hours (~2 weeks). The top sub-plot shows the erosion rate as a function of operating hours for the simulated test (black dots) and curve fits to the SPT-100 data (blue solid line). The bottom sub-plot shows the eroded volume as a function of operating hours for the simulated test (black dots) and the curve fits to the SPT-100 data (red solid line). Each black dot represents a test where LIF and CRDS data are taken. For this 4000-hour endurance test, the accelerated wear test would have reached an eroded volume of 25.1 cm³ while the real test reached ~23.3 cm³. The accelerated test overestimated the the eroded volume by ~8% and involved 15 pump-downs (there is one extra pump-down at the end to check the result at 4000 hours).

Table 1 shows the eroded volume at 4000 hours for a variety of time step sizes. The total test time for the accelerated wear test is calculated based on 2-day test cycles. This assumption is for a relative small chamber where one day would be spent modifying the channel and pumping the chamber down while the next day is spent taking data and venting the chamber. It is further assumed that there will be 5 working days per week with no testing on the weekend. Maintenance needs are assumed to be smaller given that the accelerated wear test is quite a bit shorter so the amount of time assigned to facility maintenance will be set to 15%. In contrast, the test time for a full qualification would be operated 7 days a week but with extra down time due to heavy load on the vacuum facility. The duty cycle, defined as thruster on time divided by total time, will be set to 70%.

The results shown in Table 1 are promising and illustrate an important trait of the accelerated wear test. Due to

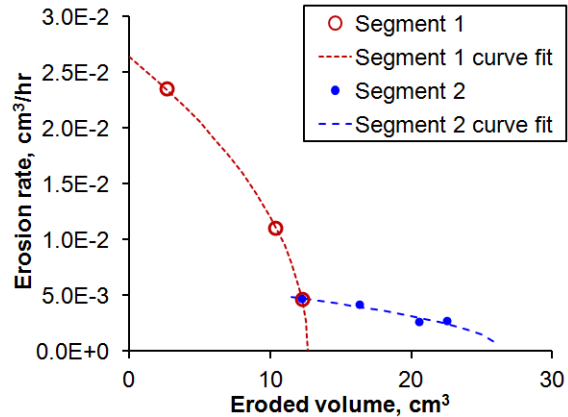


Figure 16. Erosion rate as a function of eroded volume for the SPT-100. Data calculated from Absalamov, S. K., et al.²¹

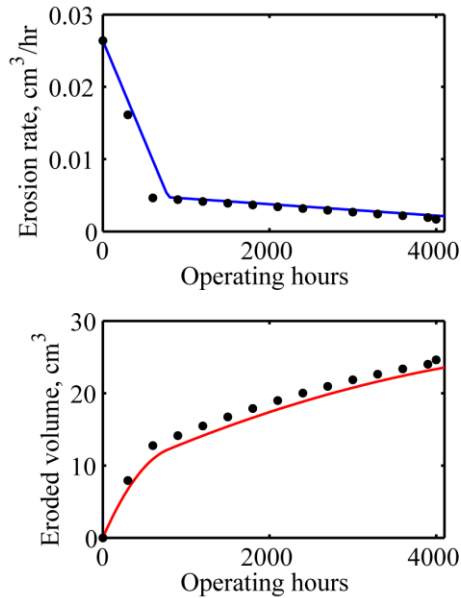


Figure 17. Results of a simulated accelerated wear test of the SPT-100 using fixed 300-hr time steps.

Table 1. Simulated accelerated wear test results compared to traditoinal wear test result.

Type	Time step size, hours	Wear time, hours	Number of sub-tests	Eroded volume, cm ³	Percentage difference	Total test time, weeks
Accelerated	200	4000	21	24.3	4.3%	9.9
Accelerated	300	4000	15	25.1	7.7%	7.1
Accelerated	400	4000	11	25.4	9.0%	5.2
Accelerated	500	4000	9	25.6	9.9%	4.2
Traditional	-	4000	-	23.3	-	34.0

the monotonically decreasing nature of the erosion rate versus time, the accelerated wear test will always overestimate the eroded volume (underestimate the life time). While any error is undesirable, it is good from an engineering perspective that the accelerated wear test will always err on the side of caution. Furthermore, we can see from Table 1 that the error is quite small. Even for a 500-hr time-step accelerated wear test the overestimate in eroded volume is only ~10% while the total test time is a mere 4 weeks compared to the 34 weeks needed for a traditional wear test.

No measurement is without noise. While the above analysis shows promising results, it was performed assuming perfect measurement accuracy. We will now introduce varying amount of noise into the measurement and see how the results vary. Figure 18 shows a case of simulated accelerate wear test where the CRDS sensor has a measurement uncertainty of $0.002 \text{ cm}^3/\text{hr}$ with a 95% confidence interval (95% C.I.). The top sub-plot shows the erosion rate as a function of operating hours for the simulated test (black dots) and curve fits to the SPT-100 data (blue solid line). The bottom sub-plot shows the eroded volume as a function of operating hours for the simulated test (black dots) and the curve fits to the SPT-100 data (red solid line). This figure shows another interesting trait of the accelerated wear test. The erosion rate measured by the accelerated wear test is “self-correcting” in the presence of measurement noise. If the erosion rate was measured to be too high, the increase in materials removed from the discharge channel cause the erosion rate measured at the next time step to drop below the actual value, and vice versa. Thus, even in the presence of noise, the eroded volume as a function of operating time for the accelerated wear test tracks very well with the traditional wear test results.

Table 2 shows how the result of the accelerated wear test vary with uncertainty in the erosion rate measurement. Even with a measurement uncertainty of $0.002 \text{ cm}^3/\text{hr}$, the eroded volume can be predicted with a precision of ~5%. Incidentally, the measurement sensitivity of the CRDS setup used during the initial demonstration described in a previous section has a peak sensitivity of $\sim 0.002 \text{ cm}^3/\text{hr}$.⁴ That is to say if sensitivity is the only limiting issue, the initial demonstration CRDS sensor is already good enough for use in an accelerated wear test of the SPT-100. With that said, the initial demonstration test identified a number issues like mirror degradation, ionization of sputtered boron, and boron velocity prediction that still needs to be worked on before CRDS is able to provide accurate measurements. Furthermore, sensitivity of the CRDS sensor does need to be improved for measuring the sputtered rate of state-of-the-art Hall thrusters, which are designed to have much lower sputter rate than the SPT-100. Nevertheless, the use of CRDS for obtaining accelerated wear test data is very promising. Work on improving the CRDS sensor is ongoing and the possibility of significantly improved sensitivity over the initial demonstration unit has already been observed.²²

Other diagnostics that can potentially be used to measure discharge channel erosion rate in near-real-time include multi-layer embedded marker,²³ emission spectroscopy,²⁴ and radioactive tracer.²⁵ Each technique has its advantages and disadvantages that will not be explored in this paper.

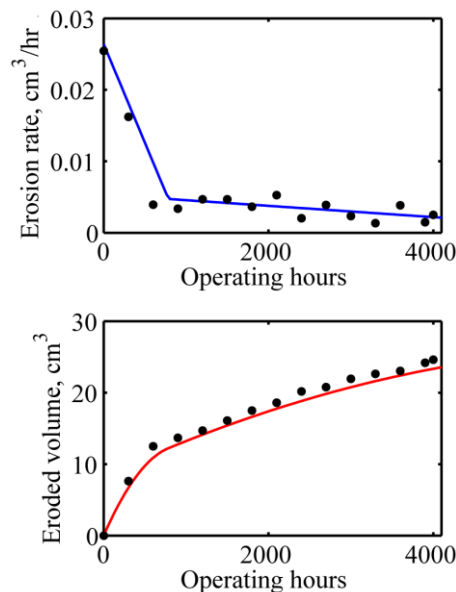


Figure 18. Results of a noisy simulated accelerated wear test of the SPT-100 using fixed 300-hr time steps. The uncertainty in the CRDS measurement is $\pm 0.002 \text{ cm}^3/\text{hr}$.

Table 2. Sensitivity of simulated accelerated wear test result to measurement uncertainty.

Measurement uncertainty (95% C.I.), cm^3/hr	Time step size, hours	Wear time, hours	Average eroded volume, cm^3	Relative uncertainty in eroded volume (95% C.I.), cm^3
0.0005	300	4000	25.1	1.3%
0.001	300	4000	25.1	2.6%
0.002	300	4000	25.1	5.1%

V. Cost Saving Estimates

This section will provide a rough comparison of the cost associated with a traditional long duration wear test versus an accelerated wear test. For this paper, the cost will cover only the operational part of the tests (no initial setup cost, no post-test analysis and tear down cost). The first cost estimate example will be on a thruster like the SPT-100 running at a xenon flow rate of 5.2 mg/s. The test is set to terminate at 4000 wear hours. The facility cost is set to \$15,000 per week and includes facility operation, maintenance, and associated personnel. The xenon will be recycled at a cost of \$2 per liter. A researcher will be assigned to the test at half-time for the traditional test and full-time for the accelerated test at a paid rate of ~\$1500 per week. For the traditional test, the thruster is operated 70% of real time while 30% of real time is spent on maintenance. For the accelerated test, the time step is 300 hours, each sub-test requires 5 hours of operation time, and 15% of the real time is spent on maintenance. These estimates are arbitrary and are only meant to give the reader a rough feel for the cost. No overhead is assigned since overhead varies greatly with organization. Note that thruster operation time, wear time, and real time are different. Operation time is the duration of thruster operation. Wear time is the effective number of hours the discharge channels have been worn. Real time is time in the real world. The facility/personel cost is multiplied by real time while the propellant cost is multiplied by thruster operation time.

The second cost estimate example will be on a 20-kW thruster designed to last 10,000 operating hours. This thruster will have a xenon flow rate of 60 mg/s. We will assume the erosion rate profile for this thruster is like the SPT-100 except scaled to 10,000 hours instead of 4000 hours. Thus, the number of sub-tests for this accelerated test will still be 15. Pump-down frequency for the accelerated wear test is now reduced to once per week because the associated vacuum facility for high-power Hall thruster testing is correspondingly larger. The cost of this larger facility will be set to \$30,000 per week and the number of researchers is increased to 2 for better redundancy.

Table 3 shows the result of the rough cost calculations for both example thrusters. For the SPT-100, the cost of discharge channel wear testing is reduced by a factor of five if performed using the accelerated approach as opposed to the traditional approach. For the 20-kW Hall thruster, the cost is reduced by a factor of six. For both thruster, the real time spent on the wear test is reduced by a factor of five. Since the setup and tear down cost is not accounted for, the real percentage of savings will not be as great. Nevertheless, the amount of time and resources saved by performing an accelerated wear test as opposed to a traditional wear test is very large.

VI. Potential Weaknesses

Ultimately, time cannot be completely cheated. The accelerated wear test does not provide exactly the same information as a traditional wear test. The biggest drawback of the approach to accelerated wear test described in this paper is that it does not wear test components other than the discharge channels. Thus, if only the accelerated wear test is performed, some other factor (like flight heritage) is being relied on to qualify components other than the discharge channels.

A second potential weakness for the accelerated wear test approach described in this paper is that the use of straight chamfer assumption may lead to added uncertainties in the results. These uncertainties can be corrected over time as more knowledge is gained on how the erosion profile should be shaped.

A third potential weakness is that, at the present time, it is not clear whether a freshly cut boron nitride surface will erode the same way as a surface that was created purely by erosion. If this is an issue, a potential work-around would be to run the thruster for some extra hours during each sub-test to ensure the thruster has a roughened surface. However, the work-around increases test cost and time.

A fourth potential weakness is that the approach does not simulate the grooves that typically form in the erosion band. The depth of the grooves can lead to local breaches in the channel walls earlier than expected. This issue can potentially be resolved by adding extra margin to the prediction from the accelerated wear test.

Table 3. Rough cost estimates of traditional versus accelerated wear tests.

Type	Thruster	Wear time, hours	Number of sub-test	Operation time, hours	Real time, weeks	Total cost
Accelerated	SPT-100	4000	15	75	7.1	\$118,000
Traditional	SPT-100	4000	-	4000	34	\$561,000
Accelerated	20-kW	10000	15	75	17.6	\$586,000
Traditional	20-kW	10000	-	10000	85	\$3,410,000

VII. Other applications

The optical diagnostics and methodology described in this paper has other life-time-characterization-related applications. For instance, the technique used in qualitative life time assessment (phase I) can also be used to fine tune the settings of the Hall thruster prior to long duration wear testing. Due to the non-intrusive and real-time nature of the LIF measurement, it is possible to perform parametric studies of how the erosion zone changes with controls like the magnetic field settings. Performing this fine tuning task on a thruster can improve its chance of passing the life time qualification test as well as give confidence that the qualification test will succeed. Even if the tuning turns out to be unnecessary, the reduction in risk associated with knowing that the erosion zone is properly placed may become the needed justification for initiating a wear test.

The quantitative life time assessment (phase II) technique presented in this paper also has other useful applications. This technique allows quick re-qualification of a qualified thruster for new mission profiles and operating conditions. Normally, this qualification process can only be bypassed if the researcher can prove that the new profile/condition will produce equal or lower wear on the discharge channels than the qualified profile/condition. However, it is not always possible to determine, in advance, future mission needs. Accelerated wear test is well suited for this type of situation where the discharge channel is the only component that really needs re-qualification and the budget is likely limited.

The ability to re-qualify thruster rapidly is also useful for building a set of branching scenarios for a given mission. If we assume, as we did for phase II, that erosion rate is the same regardless of how one arrives at a channel profile, we can create multiple scenario branches and restart the qualification process at the head of each branch. For example, suppose the Dawn mission designers wants to know how a Hall thruster will hold out if the Dawn spacecraft goes to Pluto instead of Ceres after Vesta. This could happen if spacecraft condition after reaching Ceres is uncertain and a decision cannot be prior to launch. The mission scenario now has two branches, one where Dawn visits Vesta then Ceres, and the other where Dawn visits Vesta then Pluto. The qualification test can be carried out using the mission profile for the first branch, and then restart right after the Vesta leg of the mission and complete another qualification test through the remainder of the second branch. This process is accomplishable with the traditional wear test approach, but is prohibitively expensive in cost and time. The accelerated wear test approach greatly reduces both cost and time, thereby enabling the study of branching scenarios for wear testing. This study can greatly increase mission design flexibility.

VIII. Conclusion and Future Work

This paper described two optical diagnostics used in novel fashions to enable accelerated wear testing of Hall thruster discharge channel walls. The associated analysis demonstrated factors of 5-6 savings in cost and time when an accelerated wear test is performed instead of a traditional wear test. Simulations demonstrated two interesting traits of the accelerated wear test. The accelerated wear test always underestimate the channel wall life time, though not by much, and the process is self-correcting in the presence of noise. The analysis further showed that the sensitivity level of the CRDS sensor used during the initial feasibility demonstration is high enough to predict the eroded volume of the discharge channel of the SPT-100 with a precision of ~5% after 4000 wear hours.

Assumptions and weaknesses of the accelerated wear test approach are described. The biggest weakness identified by the paper is the fact that the accelerated wear test does not wear test any component other than the discharge channel walls. Nevertheless, the described approach is very promising based on the amount of resource savings predicted by the cost analysis.

Acknowledgments

We thank Dr. Mitat Birkan of the Air Force Office of Scientific Research (AFOSR) for grant FA9550-06-1-0105 and FA9550-07-1-0535 that funded the LIF and CRDS work. We also thank Dr. Hani Kamhawi and the Glenn Research Center for support via the NASA Graduate Student Researchers Program, grant NNX09AK99H.

References

- ¹Dankanich, J. W., Kamhawi, H., and Mathers, A. J., "HiVHAC Maximum Operating Power Mission Impacts", *31st International Electric Propulsion Conference*, 2009-213, Ann Arbor, MI, 20-24 Sep., 2009.
- ²Kamhawi, H., Haag, T. W., Jacobson, D. T., and Manzella, D. H., "Performance Evaluation of the NASA-300M 20 kW Hall Effect Thruster", *47th AIAA/ASME/SAE/ASEE Joint Propulsion Conference & Exhibit*, AIAA-2011-5521, San Diego, CA, 31 Jul.- 3 Aug., 2011.
- ³Huang, W., Gallimore, A. D., and Smith, T. B., "Two-Axis Laser-Induced Fluorescence of Singly-Charged Xenon inside a 6-kW Hall Thruster", *49th AIAA Aerospace Sciences Meetings*, AIAA-2011-1015, Orlando, FL, 4-7 Jan., 2011.

- ⁴Huang, W., Gallimore, A. D., Smith, T. B., Tao, L., and Yalin, A. P., "Initial Cavity Ring-Down Density Measurement on a 6-kW Hall Thruster", *47th AIAA/ASME/SAE/ASEE Joint Propulsion Conference & Exhibit*, AIAA-2011-5994, San Diego, CA, 31 Jul.- 3 Aug., 2011.
- ⁵Peterson, P. Y. and Manzella, D. H., "Investigation of the Erosion Characteristics of a Laboratory Hall Thruster", *39th AIAA/ASME/SAE/ASEE Joint Propulsion Conference & Exhibit*, AIAA-2003-5005, Huntsville, AL, 20-23 Jul., 2003.
- ⁶Misuri, T., Milani, A., and Andrenucci, M., "Development of a Telemicroscopy Diagnostic Apparatus and Erosion Modelling in Hall Effect Thrusters", *31st International Electric Propulsion Conference*, 2009-036, Ann Arbor, MI, 20-24 Sep., 2009.
- ⁷Arhipov, B. A., et al., "The Results of 7000-Hour SPT-100 Life Testing", *24th International Electric Propulsion Conference*, IEPC-1995-039, Moscow, Russia, Sep., 1995.
- ⁸Garner, C. E., Brophy, J. R., Polk, J. E., and Pless, L. C., "A 5,730-Hr Cyclic Endurance Test of the SPT-100", *31st AIAA/ASME/SAE/ASEE Joint Propulsion Conference*, AIAA-1995-2667, Pasadena, CA, 10-12 Jul., 1995.
- ⁹Cornu, N., Marchandise, F., Darnon, F., and Estublier, D., "The PPS1350-G Qualification Demonstration: 10500 hrs on the Ground and 5000 hrs in Flight", *43rd AIAA/ASME/SAE/ASEE Joint Propulsion Conference & Exhibit*, AIAA-2007-5197, Cincinnati, OH, 8-11 Jul., 2007.
- ¹⁰de Grys, K., Mathers, A., Welander, B., and Khayms, V., "Demonstration of 10,400 Hours of Operation on a 4.5 kW Qualification Model Hall Thruster", *46th AIAA/ASME/SAE/ASEE Joint Propulsion Conference & Exhibit*, AIAA-2010-6698, Nashville, TN, 25-28, Jul., 2010.
- ¹¹Huang, W., Smith, T. B., and Gallimore, A. D., "Obtaining Velocity Distribution using a Xenon Ion Line with Unknown Hyperfine Constants", *40th AIAA Plasmadynamics and Laser Conference*, AIAA-2009-4226, San Antonio, Texas, 22-25 Jun., 2009.
- ¹²Huang, W., "Study of Hall Thruster Discharge Channel Wall Erosion via Optical Diagnostics", Ph.D. Dissertation, Aerospace Engineering, University of Michigan, Ann Arbor, MI, 2011.
- ¹³Huang, W., Drenkow, B., and Gallimore, A. D., "Laser-Induced Fluorescence of Singly-Charged Xenon Inside a 6-kW Hall Thruster", *45th AIAA/ASME/SAE/ASEE Joint Propulsion Conference & Exhibit*, AIAA-2009-5355, Denver, CO, 2-5 Aug., 2009.
- ¹⁴Berden, G., Peeters, R., and Meijer, G., "Cavity ring-down spectroscopy: Experimental schemes and applications", *International Reviews in Physical Chemistry*, Vol. 19, No. 4, 2000, pp. 565-607.
- ¹⁵Ngom, B. B., Smith, T. B., Huang, W., and Gallimore, A. D., "Numerical Simulation of the Zeeman Effect in Neutral Xenon from NIR Diode-Laser Spectroscopy", *Journal of Applied Physics*, Vol. 104, No. 2, doi:10.1063/1.2955761, 23 Jul., 2008, pp. 023303.
- ¹⁶Garnier, Y., Viel, V., Roussel, J. F., and Bernard, J., "Low-energy xenon ion sputtering of ceramics investigated for stationary plasma thrusters", *Journal of Vacuum Science and Technology*, Vol. 17, No. 6, doi:10.1116/1.582050, Nov/Dec, 1999, pp. 3246-3254.
- ¹⁷Rubin, B., Topper, J. L., and Yalin, A. P., "Total and differential sputter yields of boron nitride measured by quartz crystal microbalance", *Journal of Physics D: Applied Physics*, Vol. 42, No. 20, doi:10.1088/0022-3727/42/20/205205, 23 Sep., 2009, pp. 205205.
- ¹⁸Gamero-Castano, M. and Katz, I., "Estimation of Hall Thruster Erosion using HPHall", *29th International Electric Propulsion Conference*, IEPC 2005-303, Princeton, NJ, 31 Oct. - 4 Nov., 2005.
- ¹⁹Shastry, R., "Experimental Characterization of the Near-Wall Region in Hall Thrusters and its Implications on Performance and Lifetime", Ph.D. Dissertation, Aerospace Engineering, University of Michigan, Ann Arbor, MI, 2011.
- ²⁰Morozov, A. I., "Focussing of Cold Quasineutral Beams in Electromagnetic Fields", *Soviet Physics Doklady*, Vol. 10, No. 8, Feb., 1966, pp. 775-777.
- ²¹Absalamov, S. K., et al., "Measurement of Plasma Parameters in the Stationary Plasma Thruster (SPT-100) Plume and Its Effect on Spacecraft Components", *28th AIAA/ASME/SAE/ASEE Joint Propulsion Conference*, AIAA-1992-3156, Nashville, TN, 6-8 Jul., 1992.
- ²²Lee, B. C., Tao, L., Taylor, J. M., Yalin, A. P., and Gallimore, A. D., "Sensitivity Improvements to Laser Sensor for Boron Nitride Erosion in Hall Thrusters", *32nd International Electric Propulsion Conference*, 2011-068, Wiesbaden, Germany, 11-15 Sep., 2011.
- ²³Cho, S., et al., "Hall Thruster Channel Wall Erosion Rate Measurement Method Using Multilayer Coating Chip", *46th AIAA/ASME/SAE/ASEE Joint Propulsion Conference & Exhibit*, AIAA-2010-6697, Nashville, TN, 25-28 Jul., 2010.
- ²⁴Pagnon, D., Balika, L., and Pellerin, S., "QCM and OES: two ways used to study simultaneously HET thruster chamber ceramic erosion. First QCM results on PPS100-ML validate previous OES measurements.", *31st International Electric Propulsion Conference*, 2009-118, Ann Arbor, MI, 20-24 Sep., 2009.
- ²⁵Polk, J. E., Jaskowsky, W. v., Kelley, A. J., and Jahn, R. G., "Measurement of MPD Thruster Erosion Using Surface Layer Activation", *Journal of Propulsion and Power*, Vol. 3, No. 1, Jan - Feb, 1987, pp. 33-38.